Express Polymer Letters Vol.17, No.1 (2023) 29–39
Available online at www.expresspolymlett.com
https://doi.org/10.3144/expresspolymlett.2023.3

Research article

Interphase percolation phenomena in chitosan-graphene oxide nanocomposites, the role of water content

Yevgen Prokhorov[*], *Gabriel Luna-Barcenas*, *Yuriy Kovalenko*

Cinvestav, Unidad Querétaro, 76230 Querétaro, QRO, Mexico

Received 14 April 2022; accepted in revised form 17 August 2022

Abstract. Herein, we report interphase percolation phenomena in chitosan-graphene oxide (CS-GO) nanocomposites as a function of water content. The dependencies of the DC conductivity and the static dielectric constant have been investigated in a wide range of GO concentrations (0–12 wt%) and water contents (0, 4, 9, and 24%). Fourier-transform infrared spectroscopy (FTIR), Raman spectroscopy and X-ray diffraction (XRD) measurements reveal the presence of strong interaction between the CS matrix and GO fillers. For annealed CS-GO films in a vacuum (no water content), the DC conductivity and dielectric constant do not depend upon the GO concentration. When the water content increases, a percolation phenomenon is now detected; by increasing water content, the percolation threshold shifts to a lower GO concentration. A three-phase model which includes the conductivities of CS and GO, and an interphase layer fits well DC conductivity data; this model-based analysis suggests that upon increasing the water content, the conductivity of the interphase layer is higher than the one of both neat CS and GO. Water molecules at the interface drive a high-conductivity interfacial shell supporting a proton transfer mechanism; this mechanism is a plausible scenario for percolation in wet CS-GO nanocomposites. Our results may be of great importance in the applications of such nanocomposites in flexible electronics, biomedicine, proton exchange membranes, and sensors.

Keywords: *nanocomposites, biocomposites, material testing, percolation, interphase layer*

1. Introduction

In the last decade, chitosan-graphene oxide (CS-GO) nanocomposites have been extensively studied in different research fields for applications in biomedicine [1], adsorption of various water pollutants [2], food packaging [3], biosensing [4], proton exchange membranes [5], pharmacology [6], organic electronics [7], *etc*. Such wide applications are related to good film-forming capability, biocompatibility, excellent mechanical properties, and proton conductivity. Additionally, graphene oxide contains carboxyl and epoxy groups that help GO disperse readily in aqueous media; its surface is negatively charged due to an apparent ionization of carboxylic acid and phenolic hydroxyl groups on the GO sheets [8]. When CS dissolves in acids NH_3^+ groups form and adhere to negatively charged GO surfaces. Therefore, the surface groups of GO can interact with the CS matrix via hydrogen bonding and electrostatic interactions to achieve good dispersion [9]. Both CS and GO are hydrophilic materials with high proton conductivity due to proton hopping among hydrogen-bonding networks along the adsorbed water via Grotthus and/or vehicle mechanisms [9]. Moreover, the proton conductivity of GO can reach up to 10^{-2} S/cm [10]. Consequently, the addition of graphene oxide in a CS matrix tends to increase proton conductivity, and a percolation effect may be observed as in the case of other GO-polymer based membranes [10–12].

The conductivity percolation effect is related to an abrupt increase in conductivity upon increasing fillers concentration and an eventual saturation. On the other

[*]Corresponding author, e-mail: prokhorov@cinvestav.mx

hand, the dielectric constant ε of a percolating system increases before the percolation threshold according to power-law dependence [13, 14]. However, in the literature percolation effect has only been reported for CS-poly(vinyl pyrrolidone)-polycarboxylate functionalized graphene nanoplates with a percolation threshold at 25 wt% of graphene nanoplates [15], CS-polymetanitroaniline-functionalized graphene with a percolation threshold at 3.5 vol% [16], and CS-GO functionalized with sulphonic acid with a percolation threshold at 0.49 wt% [17]. Conversely, in CS-bio-functionalized graphene [18] and CS-sulfonated GO [19] the percolation effect has not been observed.

Additionally, the values of dielectric constant (ε) of CS-GO nanocomposites reported in the literature exhibit large dispersion. For example, at the frequency of 1 kHz, in ref. [20] for CS-GO (with 4 wt% of GO) $\varepsilon \approx 1$; in ref. [21] for 2 wt% of GO $\varepsilon \approx 0.45$ and in CS-GO functionalized with sulphonic acid [16] for 0.08 volume fraction of GO ε can reach 3500.

It is well known that the conductivity and the dielectric constant of CS-GO nanocomposites strongly depend upon water content [19]. However, to the best of our knowledge, in the literature, there are no reports on how water content will affect the percolation properties of CS-GO nanocomposites. The knowledge about the influence of water on the percolation properties of such nanocomposites plays an essential role in a variety of applications, including the development of proton exchange membranes, sensors, organic electronics, and in biomedicine; the conductivity and dielectric constant of nanocomposites affect their biocompatibility [22].

Based on the above discussion, the aim of this work is to investigate the percolation phenomena associated with CS-GO nanocomposites in a wide range of GO concentrations and under different water content. Additionally, Fourier-transform infrared spectroscopy (FTIR), Raman spectroscopy and X-ray diffraction (XRD), weight, and dielectric spectroscopy measurements were carried out to shed light on the properties of wet CS-GO nanocomposites for many different modern applications.

2. Experimental

Chitosan (CS, medium molecular weight, deacetylation 75–85%), acetic acid (99.7%), and graphene oxide sheets dispersed in water were purchased from Merck (Mexico). All the reagents were of analytical grade.

1 g of chitosan was dissolved in 99 ml of a 0.1 M acetic acid solution with subsequent stirring to promote dissolution. Different amounts of colloidal GO suspensions were sonicated (0–12 wt% GO, CS dry base) and dispersed in the CS solution by ultrasound for 60 min. Nanocomposite films (with a thickness of about 30–60 μm) were prepared by the solvent cast method by pouring the solution into a plastic Petri dish and allowing the solvent to evaporate at 60 °C for 24 hours. A thin layer of gold was sputtering onto both sides of the film previously to electrical measurements to serve as electrodes.

FTIR measurements were carried out on a Perkin Elmer Spectrum spectrophotometer (USA) using an attenuated total reflection (ATR) accessory in the range 4000–650 cm^{-1} and with a resolution of 4 cm^{-1}. Raman spectroscopic measurements were carried out using a Dilor Labram II (USA) with an excitation laser of 632.8 nm.

XRD measurements were performed using a Rigaku diffractometer ULTIMA IV (Japan), equipped with Cu K_α radiation (l = 1.5406 Å).

Impedance measurements were carried out on films with different water content in air and vacuum at room temperature using Agilent 4249 A (USA) in the frequency range 40 Hz–70 MHz with an amplitude of AC voltage 100 mV. DC resistance R and capacitance C at the limit of zero frequency were calculated from fitting impedance spectra using ZView® program (USA). Conductivity (σ) and static dielectric constant (ε_s) (at the limit of zero frequency) were calculated from the following relationship: $\sigma = d/(R \cdot S)$, $\varepsilon_s = (C \cdot d)/(\varepsilon_0 \cdot S)$, where d and S are the thickness and area of samples, respectively. Film thickness was measured in each sample using a micrometer Mitutoyo (Japan) with a resolution of 1 μm.

The water content of CS–GO films was determined by measuring the change in weight between the dry and wet films using Sartorius AZ214 analytical balance (USA) with readability of 0.0001 gm. Weight of dry films (W_d) was obtained on films annealing to the temperature of 120 °C in a vacuum cell for 1 hour, followed by cooling to room temperature for further measurements. Due to water absorption, the weight of CS–GO films changes when compared with those annealed. Moisture content (W [%]) was calculated using the Equation (1):

$$W\,[\%] = \frac{W_0 - W_d}{W_0} \tag{1}$$

where W_0 is the sample weight measured after the different treatments.

As the prepared films have a water content *ca*. 9%. The nanocomposite films soaked in a vacuum at 25 °C for 30 min. have a water content *ca*. 4%. For higher water content, samples were placed in a home-made water chamber bath with deionized water at 80 °C for 40 min – exposure time. This conditioning time allows one to obtain *ca*. 24% of water.

3. Results and discussion

FTIR spectrum of GO [23, 24] and neat CS [25] are consistent with previous reports in the literature. Figure 1 shows the FTIR spectra of GO, neat CS films, and CS-GO films with 7 and 12 wt% of GO. For GO, observed broadband in the 3700–2300 cm^{-1} corresponds to the stretching vibrations of structural OH groups and water molecules. The peak at 1729 cm^{-1} is attributed to the presents of C=O stretching vibration, and the peak at 163 cm^{-1} can be assigned to the C–C stretching and absorbed hydroxyl groups in the GO. In the case of chitosan, the characteristic broadband peak centered at 3328 cm^{-1} corresponded to the overlap of stretching vibration of NH and OH groups. Additionally, it was observed the characteristic peaks at 1647 (amide I group) and 1557 cm^{-1} (bending vibrations of NH_3). The change positions of peaks in CS-GO films from 3328 to 3225 cm^{-1}; 1647 to 1625 cm^{-1}, and 1557 to 1545 cm^{-1}, and the appearance of the weak peak of GO (at 1729 cm^{-1}) can be related to the synergetic effect of electrostatic interaction between polycationic CS and the negative charge on the surface of GO and hydrogen bond between CS and oxygen-containing functional groups in GO [20, 26].

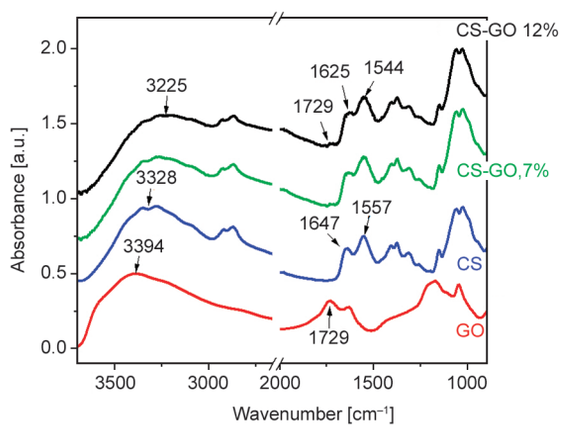

Figure 1. FTIR spectra of GO, CS, and CS-GO with 7 and 12 wt% of GO.

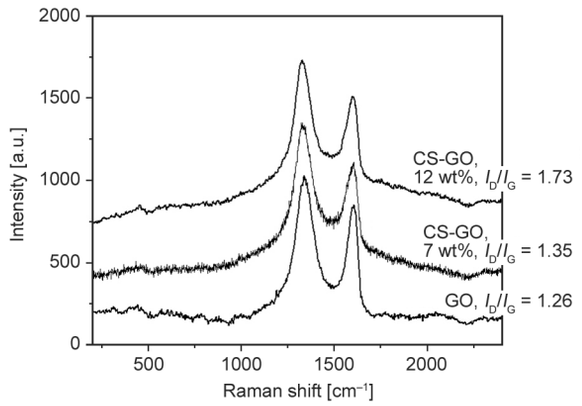

Figure 2. Raman spectra of the GO and as-prepared CS-GO films with 7 and 12 wt% of GO.

Raman measurements may be used to provide further support for the relationship between CS and GO. Figure 2 shows the Raman spectra of the GO and the prepared CS-GO films with 7 and 12 wt% of GO. The D-band (1330 cm^{-1}), which may be attributed to a defect or a disordered lattice, and the G-band (1600 cm^{-1}), which is the first order scattering of the E2g mode of sp^2 domains, are present in all spectra [27]. Typically, the I_D/I_G intensities ratio may be used to gauge the severity of structural abnormality [28]. The I_D/I_G intensity ratio for tidy GO is 1.26. In CS-GO films, this ratio rises to 1.35 for films with 7 weight percent of GO and 1.73 for films with 12 weight percent. Such a change in the D/G intensity can be attributed to the destruction of the GO layer structure and/or to the appearance of structural defects due to the interaction of GO with CS side groups [20, 27].

Moreover, the interaction between CS and GO has been observed in XRD measurements. Figure 3 shows XRD patterns of GO, neat CS, and CS-GO films

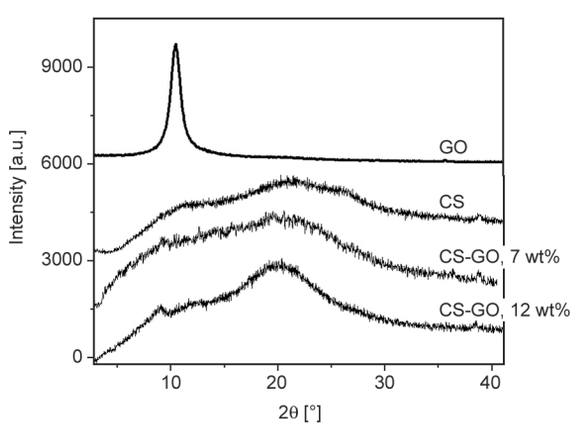

Figure 3. XRD patterns of GO, CS, and CS-GO (with 7 and 12 wt% of GO) films.

with 7 and 12 wt% of graphene oxide. The XRD pattern of GO displays a single diffraction peak at 2θ = 10.1° that corresponds to an interlayer spacing d = 8.747 Å, characteristic of neat GO [29]. The CS typically has a wide diffraction peak at 2θ = 11.5° and 2θ = 21.5° due to a combination of amorphous and crystalline phases [25, 30]. The incorporation of GO affected the crystalline structure of CS and increased the intensity of broad characteristic peaks of CS at *ca*. 21.5°. Additionally, in CS-GO films with 7 wt% of GO, a weak GO peak at 2θ = 9.1950 is observed, which is attributed to increasing GO interlayer spacing to d = 9.61 Å and in CS-GO with 12 wt% this peak shift to 2θ = 8.77° which corresponds to interlayer spacing 10.079 Å. The increasing GO layer spacing is related to the attachment of CS chains to the surface of stacked graphene nanosheets, which disrupts the van der Waals interactions and enlarges the d-spacing of the nanosheets [31]. During of film drying process, GO also affected the formation of the CS hydrogen bond, which led to a change in the crystalline structure of chitosan [30].

The results obtained from FTIR, Raman, and XRD measurements suggest that there exist strong interactions between the CS matrix and GO fillers which allow for obtaining good dispersion of GO in CS matrix.

Figure 4 illustrates the relationship between the imaginary part of impedance (Z'') and the real part of impedance (Z') (or impedance spectra) obtained on films (containing 5 wt% GO) after annealing in a vacuum cell for an hour, cooling to room temperature for measurements at 25 °C (0% water, indicated on the graph), and treatment in a water bath (*ca*. 24 percent of water). Insert displays the impedance spectra of CS-GO film that contains 12 wt% GO and 24 weight percent water.

In dry CS–GO films (annealed before measurements at 120 °C), enough bonded water exists to support proton conductivity because complete removal of water from CS is only possible by heating it to temperatures *ca*. 200 °C, where CS irreversibly transforms into an annealed polymorph [32].

As one can see, impedance spectra consist of a depressed semicircle and growth part at the low-frequency range which is related to contact and Maxwell–Wagner–Sillars (MWS) effects. MWS mechanism appears due to charge accumulation at the interface of CS and GO, as the current could not flow freely across it. As it is clear from Figure 4 that the frequency at which begin observed MWS effect dependent on GO wt% and water content [7, 33]. Consequently, measurements of dielectric constant ε at a fixed frequency, often used in the literature, did not allow to obtain real dependence of ε on GO concentration. Therefore, for separation of MWS and contact effects, we take into consideration only bulk properties of nanocomposite which are related to a depressed semicircle and fit the semicircle using the ZView program to zero frequency to calculate DC resistance and static dielectric constant at the limit of zero frequency as was shown on Figure 4.

According to percolation theory [13, 14], the power-law behavior of DC conductivity (σ_{DC}) above (Equation (2)) and below the percolation threshold (Equation (3)) and static dielectric constant (ε_s) (in the

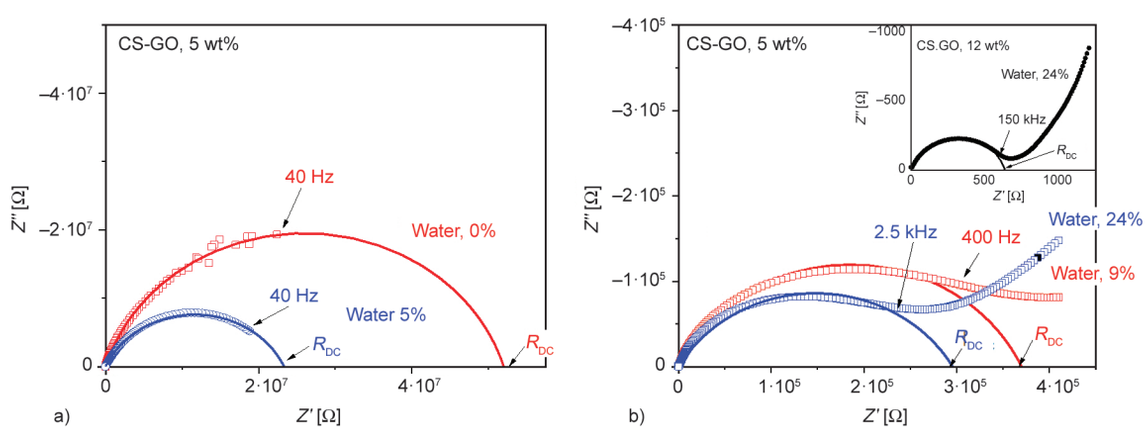

Figure 4. Impedance spectra of CS-GO films with 5 wt% of GO obtained on films with different content of water: a) with 0 and 5% of water, b) with 9 and 24% of water. Insert shows impedance spectra of CS-GO film with 12 wt% of GO and 24% of water. Note: Spectra for water 24% has been increased 100 times for better visualization. Symbols correspond to experimental points, and continuous lines represent the results of fitting using ZView program.

limit of zero frequency) below the percolation threshold (Equation (4)) can be obtained by a simple power-law:

$$\sigma_{DC} \propto (p - p_c)^t \quad \text{for} \quad p > p_c \tag{2}$$

$$\sigma_{DC} \propto (p_c - p)^{-q} \quad \text{for} \quad p < p_c \tag{3}$$

$$\varepsilon_s \propto (p_c - p)^{-s} \quad \text{for} \quad p < p_c \tag{4}$$

where t, q, and s are critical exponents which only depend upon the dimension of the percolation system and not on the details of cluster geometry, and pc is the volume fraction of fillers at the percolation threshold. Therefore, to convert the weight fraction (W_t) of GO to volume fraction (V), the Equation (5) was used [34]:

$$V = \frac{W_t}{W_t + \frac{\rho_{GO}}{\rho_{CS}}(1 - W_t)} \tag{5}$$

where ρ_{GO} = 1.7 g/cm^3 [35] and ρ_{CS} = 1.4 g/cm^3 [36] are density of GO and CS respectively.

Figure 5 shows the DC conductivity (Figure 5a) and dielectric constant in the zero-frequency limit (Figure 5b) *versus* GO volume fraction and GO wt%. In the case of CS-GO films, annealing before measurements in vacuum DC conductivity (σ_{DC}) and dielectric constant (ε_s) does not depend on the GO concentration. In samples with 4% of water with an increasing GO content ε_s riches a maximum at GO vol. frac. *ca*. 9% (or *ca*. 11wt%), and σ_{DC} increases by a power law, which is typical for the percolation effect. Figure 6a shows the log-log dependence of the dielectric constant of the CS-GO nanocomposite films on log($p_c - p$) calculated from experimental data (Figure 5), which according to Equation (4), must exhibit linearity. The least-square fitting analysis allows obtaining a percolation threshold of 9.2% vol. frac. of GO (*ca*. 11wt%) and slope q = 0.71±0.08. In films with 9 and 24% of water, the percolation effect was observed to be more apparent in conductivity (appear saturation) and dielectric constant (the maximum is more pronounced).

The least-square fitting analysis of conductivity according to Equation (2) for above the percolation threshold gave p_c = 4.5 vol% (or *ca*. 5.5 wt%) for films with 9% of water and p_c = 3.6 vol% (or *ca*. 4 wt%) for films with 24% of water and critical exponent t = 2.02±0.13 and t =1.98±0.16, respectively (Figure 6b). The best fits of the dielectric constant data below the percolation threshold (Equation (4)) gave the same values of p_c as for conductivity (4.5 and 3.6% of GO volume fraction) and critical exponent s = 0.62±0.021 and s = 0.64±0.058 for films with 9 and 24% of water respectively (Figure 6a). According to the percolation theory in three-dimensional system values t = 1.6–2.0 and s = 0.7–1.0 [13, 14]. The values of critical exponent s obtained in CS-GO films with high water content are a little lower but are near that universal one. Therefore, it is likely that wet CS-GO films exhibit a three-dimensional percolation phenomenon.

The percolation phenomena can be observed in a mixture of two materials with different conductivity, such as dielectric polymers, with the incorporation of different types of conducting fillers such as

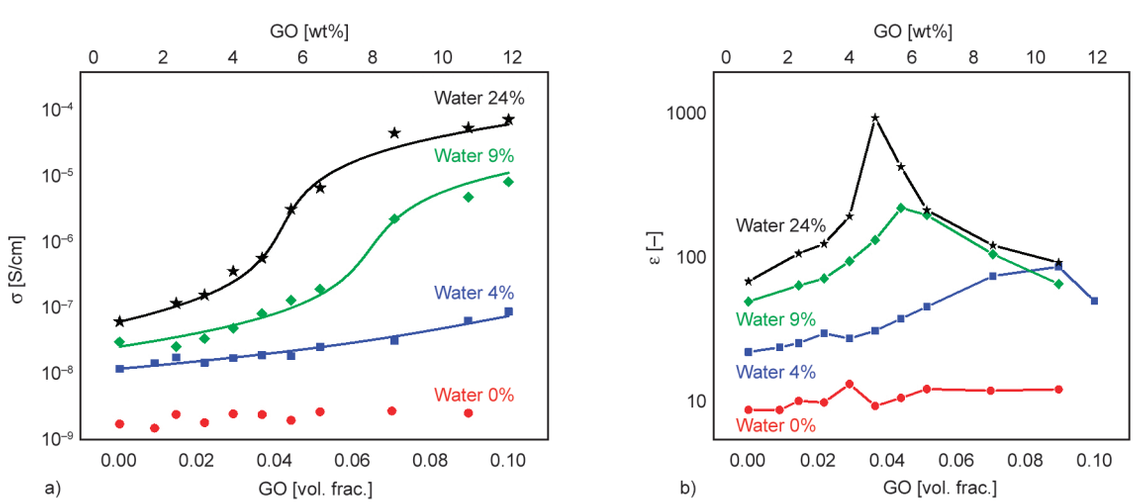

Figure 5. (a) Dependencies of conductivity (points-experimental data, continuous lines-fitting) and (b) dielectric constant as a function of GO volume fraction and GO [wt%] for films with different water content indicate on graphs.

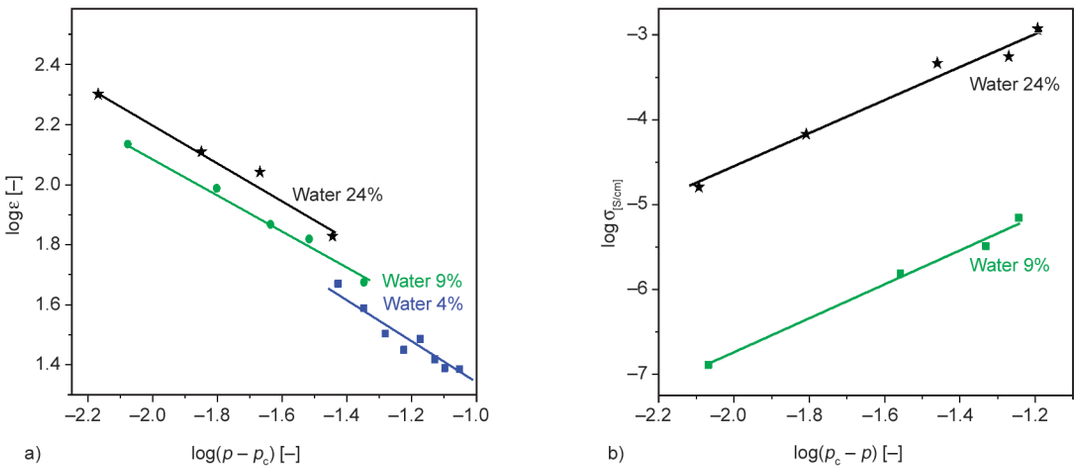

Figure 6. log-log plot of a) the dielectric constant *versus* ($p_c - p$) and b) DC conductivity *versus* ($p - p_c$). Points are experimental data, and lines are the results of the fitting.

metals, carbon fillers, conducting polymers, *etc*. In graphene-polymers composites, the percolation effect has been observed, as a rule, in nanocomposites with high conductivity graphene and its modification: graphene nanoplatelets, reduced graphene oxide, and doped GO [13]. However, to the best of our knowledge, there are no reports on how water content affects the percolation properties of CS-GO nanocomposites.

Some studies proposed that water shell models can explain the effect of water on the formation of percolative paths through the overlapping of the water layers (see, for example [37–40]), which promotes the conduction of charge carriers. However, these models predict only the percolation probability but not the dependencies of conductivity (especially in the saturation region) and the dielectric constant. Moreover, model calculations showed that for percolation networks, the thickness of the water shell must be as high as *ca*. 60 nm [38, 40].

From another viewpoint, it is well known that polymer matrices-nanofillers interphase interactions constitute a significant parameter that highly affects the nanocomposite behavior [37, 41–43], especially when the nanocomposite moves from an insulative material to a conductive because of the creation of a continual conductive network [37, 41]. The interphase consists of layers with different electrical and chemical structures distinct from the polymer matrix due to changes in the local chain conformation [37].

According to FTIR, Raman, and XRD measurements, there exist strong hydrogen-bonding interactions between the CS matrix and GO fillers in CS-GO films. Additionally, the water interaction in CS-GO nanocomposites is higher than that of pure chitosan [44] due to stabilized polymer chains [45], formation of hydrogen bonds between water molecules with side groups of GO, and hydroxyl groups of CS [44, 46].

According to molecular dynamic simulation, the conductivity of CS exhibits proton conductivity through the Grotthus mechanism, which depends upon the number of protons, hydronium ions, and water content. When the amount of water in the system increased, the proton and hydronium ions were not mainly located near the functional group of chitosan, but they were diffused throughout the water clusters [47]. The addition of GO in CS improves the proton conductivity of nanocomposites due to the increasing

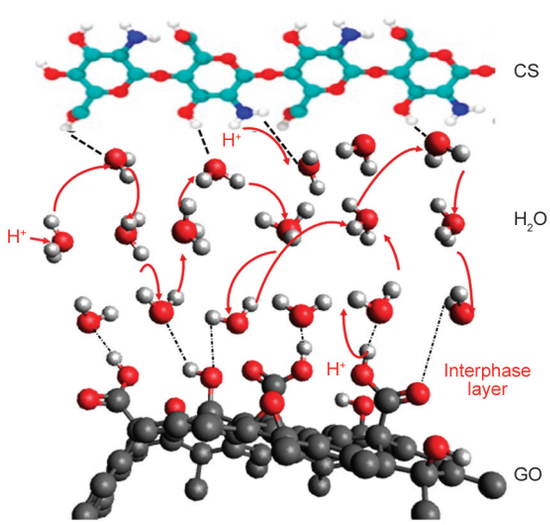

Figure 7. Schematic representation of the conductivity of wet CS-GO nanocomposite. Here, red arrows show the diffusion path of protons, and dash lines show hydrogen bonds between CS, GO and H_2O.

number of protons from carboxyl groups of GO [8] and the creation of some spatial channels; these channels facilitate the diffusion of proton and hydronium ions at the high-water content [48].

Based on the above, we can propose that the interaction of GO with CS and water molecules promotes the appearance of a high-conductivity interphase layer, as shown in Figure 7.

The protons appear from the NH_3 group of CS [47] and from carboxyl groups of GO [8] at the low water concentration located near the functional group of CS and GO. In the presence of water, the protons can diffuse through water clusters, create spatial channels, and form an interfacial layer with high conductivity (as shown in Figure 7). With increasing water content, the thickness and conductivity of the interphase layer increase due to the diffusion of proton and hydronium ions at the high-water content [48]. Therefore, the interphase provides a continuous channel for proton hopping in hydrogen-bonding networks along the adsorbed water, and it is responsible for the percolation properties of wet nanocomposites.

Direct confirmation of the proposed model can be the estimation of the conductivity and thickness of the interphase layer surrounding the GO fillers with different water content. For such an estimation, we use the model proposed in ref. [49] based on average field theory for calculating the effective conductivity of polymer-carbon nanotube composites. This model proposed that the electrical conductivity of composites depends on the concentration of fillers and the conductivity of the interphase layer. The model predicts that the percolation threshold decreases with interphase thickness and the conductivity in the saturation region increase with the interphase layer's conductivity. With increasing fillers content, the electrical conductivity of the interphase layer demonstrates a higher contribution to the effective electrical conductivity of the material.

The model has proposed that fillers can be regarded as the same rotationally prolate ellipsoids with longitude L, diameter d, and thickness of interphase layer t, which are related by the Equation (6):

$$\alpha = \frac{d^3 L}{(d+2t)^2 (L+2t)} \tag{6}$$

and effective conductivity of nanocomposite can be found from the Equation (7)) when $d \ll L$:

$$3\left(1-\frac{f}{\alpha}\right)\frac{\sigma_e-\sigma_m}{2\sigma_e+\sigma_m}+ \\ +\frac{f}{3\alpha}\left(\frac{\sigma_e-\sigma_{com}^{33}}{\sigma_e+0.14\frac{d}{L}\left(\sigma_{com}^{33}-\sigma_e\right)}\right)+4\frac{\sigma_e-\sigma_{com}^{11}}{\sigma_e+\sigma_{com}^{11}}=0 \tag{7}$$

where α is given by the Equation (6), σ_c, σ_m, σ_s, and σ_e are the electrical conductivities of the fillers, the matrix, the interphase layer, and the effective conductivity of the composite, respectively; σ_{com}^{33} and σ_{com}^{11} are the longitude and the transverse conductivity, which in the case of GO are the same.

According to the scanning electron microscopic (SEM) measurements, we estimated GO sheet dimension as $L = 3$ μm and $d = 20$ nm [50].

This model allowed us to fit not only the effective conductivity of nanocomposite but also estimated the thickness of the interphase layer, its conductivity, and the percolation threshold.

The least-squares fitting of experimental data was performed using standard genetic algorithm optimization functions in the Scilab® [51] numerical computational package. The conductivity of CS-matrix (σ_{CS}) has been obtained from measurements on neat CS films with different water content, and the conductivity of GO was taken as 10^{-4} S/cm [50]. The adjustable parameters are only the values of interfacial conductivity (σ_{inter}) and interfacial thickness (d_{inter}). Data fitting optimization parameters are presented in Table 1.

Results of the referred fittings are shown in Figure 5a as a continuous line. One can see that this three-phase model fits well the experimental results. It is noteworthy that the thickness of the interphase layer obtained from fitting correlates well with the thickness of the interfacial layer observed in other polymer nanocomposites, which is in the range of 2–6 nm [42, 43].

Table 1 shows that when the water content in CS-GO films rises, so do the conductivity and thickness of the interphase layer.

Table 1. Results of fitting experimental conductivity of CS-GO films with different water content.

Water content [%]	σ_{CS} (experimental) [S/cm]	σ_{inter} (estimated) [S/cm]	d_{inter} (estimated) [nm]
4	$1.18\cdot10^{-8}$	$9.72\cdot10^{-8}$	0.82
9	$3.06\cdot10^{-8}$	$9.58\cdot10^{-4}$	2.97
24	$6.19\cdot10^{-7}$	$4.80\cdot10^{-2}$	4.72

Additionally, due to the rise in water content, the interphase layer's conductivity in films with 9 and 24 percent water is higher than that of CS and neat GO (10^{-4} S/cm), increasing the thickness and conductivity of the interphase and facilitating proton transport at the high-water content. These findings support the suggested model's validity, showing that the strong molecular interactions of GO with CS and water molecules during the interphase between CS and GO cause the interphase to be more conductivity-rich (compared to pristine CS and GO). The percolation properties of wet nanocomposites are attributed to proton transport via hydrogen-bonding networks, which this study supports.

This result supports proton transport across hydrogen-bonding networks, which gives wet nanocomposites their percolation capabilities. In addition, as the model predicts, an increase in water content raises the conductivity and thickness of the interphase layer, which lowers the percolation threshold.

4. Conclusions

Chitosan-graphene oxide nanocomposite films were synthesized with varying GO concentrations (0–12 wt%). FTIR, Raman, and XRD measurements have shown strong interaction between the CS matrix and GO fillers which allows for obtaining good dispersion of GO in the CS matrix.

DC conductivity and dielectric constant dependencies in the zero-frequency limit have been investigated versus GO concentration and water content. In the case of CS-GO films annealing before measurements in a vacuum, DC conductivity and dielectric constant do not depend upon the GO concentration. The percolation effect has been observed, for the first time, at higher water content (4, 9, and 24%). The values of critical exponents obtained in CS-GO films with high water content allow us to conclude that nanocomposites exhibit a three-dimensional percolation system. Results of fitting DC conductivity using a three-phase model, which includes conductivity of CS, GO, and interphase layer, showed that by increasing water content in CS-GO films, the conductivity and thickness of the interfacial layer increase. Surprisingly, the conductivity of the interfacial layer in films with 9 and 24% of water is higher than the conductivity of both pristine CS and GO. The thickness of the interfacial layer increases with water content. A new percolation model for CS-GO nanocomposites with high water content has been proposed to shed light on these new findings. In this regard, we propose that due to the strong molecular interactions of GO with CS and water molecules at the interface between CS and GO, a high-conductivity interphase layer appears, which supports a proton transfer mechanism among hydrogen-bonding networks. It is responsible for the percolation properties of wet nanocomposites. Additionally, increasing water content increases the conductivity and thickness of the interphase layer, which leads to shifting the percolation threshold to lower GO concentration.

Our results here may be of great importance in the applications of such nanocomposites in different areas, not only for developing proton exchange membranes, sensors, organic electronics, and biomedicine.

Acknowledgements

This work was partially supported by CONACYT Mexico (Grant A1-S-9557). The authors acknowledge to J. A. Muñoz Salas for technical assistance in electrical measurements, F. Rodriguez Melgarejo for assistance in Raman measurements, M. Adelaido Hernandez for assistance in XRD measurements, and R.A. Mauricio Sanchez for assistance in FTIR measurements.

References

[1] Pieklarz K., Tylman M., Modrzejewska Z.: Applications of chitosan–graphene oxide nanocomposites in medical science: A review. Progress on Chemistry and Application of Chitin and its Derivatives, **XXIII**, 5–24 (2018). https://doi.org/10.15259/PCACD.23.01

[2] Ahmed M. J., Hameed B. H., Hummadi E. H.: Review on recent progress in chitosan/chitin-carbonaceous material composites for the adsorption of water pollutants. Carbohydrate Polymers, **247**, 116690 (2020). https://doi.org/10.1016/j.carbpol.2020.116690

[3] Barra A., Santos J. D. C., Silva M. R. F., Nunes C., Ruiz-Hitzky E., Gonçalves I., Yildirim S., Ferreira P., Marques P. A. A. P.: Graphene derivatives in biopolymer-based composites for food packaging applications. Nanomaterials, **10**, 2077 (2020). https://doi.org/10.3390/nano10102077

[4] Priftis D.: Polyelectrolyte-graphene nanocomposites for biosensing applications. Current Organic Chemistry, **19**, 1819–1827 (2015). https://doi.org/10.2174/1385272819666150526005557

[5] Pandey R. P., Shukla G., Manohar M., Shahi V. K.: Graphene oxide based nanohybrid proton exchange membranes for fuel cell applications: An overview. Advances in Colloid and Interface Science, **240**, 15–30 (2017). https://doi.org/10.1016/j.cis.2016.12.003

[6] Farion I. A., Burdukovskii V. F., Kholkhoev B. C., Timashev P. S., Chailakhyan R. K.: Functionalization of chitosan with carboxylic acids and derivatives of them: Synthesis issues and prospects of practical use: A review. Express Polymer Letters, **12**, 1081–1105 (2018). https://doi.org/10.3144/expresspolymlett.2018.95

[7] Feng P., Du P., Wan C., Shi Y., Wan Q.: Proton conducting graphene oxide/chitosan composite electrolytes as gate dielectrics for new-concept devices. Scientific Reports, **6**, 34065 (2016). https://doi.org/10.1038/srep34065

[8] Yang X., Tu Y., Li L., Shang S., Tao X-M.: Well-dispersed chitosan/graphene oxide nanocomposites. ACS Applied Materials and Interfaces, **2**, 1707 (2010). https://doi.org/10.1021/am100222m

[9] Yuan H., Meng L-Y., Park S-J.: A review: Synthesis and applications of graphene/chitosan nanocomposites. Carbon Letters, **17**, 11–17 (2016). https://doi.org/10.5714/CL.2016.17.1.011

[10] Cao L., Wu H., Yang P., He X., Li J., Li Y., Xu M., Qiu M., Jiang Z.: Graphene oxide-based solid electrolytes with 3D prepercolating pathways for efficient proton transport. Advanced Functional Materials, **28**, 1804944 (2018). https://doi.org/10.1002/adfm.201804944

[11] Farooqui U. R., Ahmad A. L., Hamid N. A.: Graphene oxide: A promising membrane material for fuel cells. Renewable and Sustainable Energy Reviews, **82**, 714–733 (2018). https://doi.org/10.1016/j.rser.2017.09.081

[12] Marsden A. J, Papageorgiou D. G., Vallés C., Liscio A., Palermo V., Bissett M. A., Young R. J., Kinloch I. A.: Electrical percolation in graphene–polymer composites. 2D Materials, **5**, 032003 (2018). https://doi.org/10.1088/2053-1583/aac055

[13] Stauffer D., Aharony A.: Introduction to percolation theory. Taylor and Francis, London (1992).

[14] Nan Y-C., Shen W., Ma J.: Physical properties of composites near percolation. Annual Review of Materials Research, **40**, 131–151 (2010). https://doi.org/10.1146/annurev-matsci-070909-104529

[15] Mergen O. B., Arda E., Evingür G. A.: Electrical, optical and mechanical properties of chitosan biocomposites. Journal of Composite Materials, **54**, 1497–1510 (2020). https://doi.org/10.1177/0021998319883916

[16] Pati M. K., Pattojoshi P., Roy G. S.: Synthesis of graphene-based nanocomposite and investigations of its thermal and electrical properties. Journal of Nanotechnology, **2016**, 5135420 (2016). https://doi.org/10.1155/2016/5135420

[17] Layek R. K., Samanta S., Nandi A. K.: Graphene sulphonic acid/chitosan nano biocomposites with tunable mechanical and conductivity properties. Polymer, **53**, 2265–2273 (2012). https://doi.org/10.1016/j.polymer.2012.03.048

[18] Yadav S. K., Jung Y. C., Kim J. H., Ko Y-I., Ryu H. J., Yadav M. K., Kim Y. A., Cho J. W.: Mechanically robust, electrically conductive biocomposite films using antimicrobial chitosan-functionalized graphene. Particle and Particle Systems Characterization, **30**, 721–727 (2013). https://doi.org/10.1002/ppsc.201300044

[19] Liu Y., Wang J., Zhang H., Ma C., Liu J., Cao S., Zhang X.: Enhancement of proton conductivity of chitosan membrane enabled by sulfonated graphene oxide under both hydrated and anhydrous conditions. Journal of Power Sources, **269**, 898–911 (2014). https://doi.org/10.1016/j.jpowsour.2014.07.075

[20] Dhayal A. V., Hashmi S. Z., Kumar U., Choudhary B. L., Kuznetsov A. E., Dalela S., Kumar S., Kaya S., Dolia S. N., Alvi P. A.: Spectroscopic studies, molecular structure optimization and investigation of structural and electrical properties of novel and biodegradable chitosan-GO polymer nanocomposites. Journal of Materials Science, **55**, 14829–14847 (2020). https://doi.org/10.1007/s10853-020-05093-5

[21] Dhayal V., Hashmi S. Z., Kumar U., Choudhary B. L., Dalela S., Dolia S. N., Alvi P. A.: Optical and electrical properties of biocompatible and novel (CS–GO) polymer nanocomposites. Optical and Quantum Electronics, **53**, 53 (2021). https://doi.org/10.1007/s11082-020-02723-9

[22] Chaudhuri B., Bhadra D., Moroni L., Pramanik K.: Myoblast differentiation of human mesenchymal stem cells on graphene oxide and electrospun graphene oxide–polymer composite fibrous meshes: Importance of graphene oxide conductivity and dielectric constant on their biocompatibility. Biofabrication, **7**, 015009 (2015). https://doi.org/10.1088/1758-5090/7/1/015009

[23] Krishnamoorthy K., Veerapandian M., Yun K., Kim S-J.: The chemical and structural analysis of graphene oxide with different degrees of oxidation. Carbon, **53**, 38–49 (2013). https://doi.org/10.1016/j.carbon.2012.10.013

[24] Ji W. F., Chen K. Y., Ke C. J., Liao Y. J., Liu W. J., Tsai M. H., Yeh J. M.: Comparative corrosion protection studies of electroactive/non-electroactive epoxy thermoset composites containing conductive rGO/non-conductive GO platelets. Express Polymer Letters, **13**, 604–617 (2019). https://doi.org/10.3144/expresspolymlett.2019.51

[25] Kumar-Krishnan A. S., Prokhorov E., Ramírez M., Hernandez-Landaverde M. A., Zarate-Triviño D. G., Kovalenko Y., Sanchez I. C., Méndez-Nonell J., Luna-Bárcenas G.: Novel gigahertz frequency dielectric relaxations in chitosan films. Soft Matter, **10**, 8673–8684 (2014). https://doi.org/10.1039/C4SM01804D

[26] Zuo P-P., Feng H-F., Xu Z-Z., Zhang L-F., Zhang Y-L., Xia W., Zhang W-Q.: Fabrication of biocompatible and mechanically reinforced graphene oxide-chitosan nanocomposite films. Chemistry Central Journal, **7**, 39 (2013). https://doi.org/10.1186/1752-153X-7-39

[27] Qi Y., Yang M., Xu W., He S., Men Y.: Natural polysaccharides-modified graphene oxide for adsorption of organic dyes from aqueous solutions. Journal of Colloid and Interface Science, **486**, 84–96 (2017). https://doi.org/10.1016/j.jcis.2016.09.058

[28] Sanes J., Ojados G., Pamies R., Bermúdez M. D.: PMMA nanocomposites with graphene oxide hybrid nanofillers. Express Polymer Letters, **13**, 910–922 (2019). https://doi.org/10.3144/expresspolymlett.2019.79

[29] Zhang S-B., Yan Y-T., Huo Y-Q., Yang Y., Feng J-L., Chen Y-F.: Electrochemically reduced graphene oxide and its capacitance performance. Materials Chemistry and Physics, **148**, 903–908 (2014). https://doi.org/10.1016/j.matchemphys.2014.08.068

[30] Kosowska K., Domalik-Pyzik P., Nocuń M., Chłopek J.: Chitosan and graphene oxide/reduced graphene oxide hybrid nanocomposites – Evaluation of physicochemical properties. Materials Chemistry and Physics, **216**, 28–36 (2018). https://doi.org/10.1016/j.matchemphys.2018.05.076

[31] Nath A. J., Chowdhury A., Dolui S. K.: Chitosan/graphene oxide-based multifunctional pH-responsive hydrogel with significant mechanical strength, self-healing property, and shape memory effect. Advances in Polymer Technology, **37**, 3665–3679 (2018). https://doi.org/10.1002/adv.22151

[32] Ogawa K., Yui T., Okuyama K.: Three D structures of chitosan. International Journal of Biological Macromolecules, **34**, 115-120 (2004). https://doi.org/10.1016/j.ijbiomac.2003.11.002

[33] Xia X., Zhong Z., Weng G. J.: Maxwell–Wagner–Sillars mechanism in the frequency dependence of electrical conductivity and dielectric permittivity of graphene-polymer nanocomposites. Mechanics of Materials, **109**, 42–50 (2017). https://doi.org/10.1016/j.mechmat.2017.03.014

[34] Zakaria A. Z., Shelesh-Nezhad K.: The effects of interphase and interface characteristics on the tensile behaviour of POM/$CaCO_3$ nanocomposites. International Journal of Nanomaterials, Nanotechnology and Nanomedicine, **4**, 17 (2014). https://doi.org/10.5772/58696

[35] Gong T., Lam D. V., Liu R., Won S., Hwangbo Y., Kwon S., Kim J., Sun K., Kim J-H., Lee S-M., Lee C.: Thickness dependence of the mechanical properties of free-standing graphene oxide papers. Advanced Functional Materials, **25**, 3756–3763 (2015). https://doi.org/10.1002/adfm.201500998

[36] Nunthanid J., Laungtana-anan M., Sriamornsak P., Limmatvapirat S., Puttipipatkhachorn S., Lim L. Y., Khor E.: Characterization of chitosan acetate as a binder for sustained release tablets. Journal of Controlled Release, **99**, 15–26 (2004). https://doi.org/10.1016/j.jconrel.2004.06.008

[37] Pitsa D., Danikas M.: Interfaces features in polymer nanocomposites: A review of proposed models. NANO, **6**, 497–508 (2011). https://doi.org/10.1142/S1793292011002949

[38] Hosier I. L., Praeger M., Vaughan A. S., Swingler S. G.: The effects of water on the dielectric properties of silicon-based nanocomposites. IEEE Transactions on Dielectrics and Electrical Insulation, **16**, 169–179 (2017). https://doi.org/10.1109/TNANO.2016.2642819

[39] Qiang D., Wang Y., Wang X., Chen G., Andritsch T.: The effect of filler loading ratios and moisture on DC conductivity and space charge behaviour of SiO_2 and hBN filled epoxy nanocomposites. Journal of Physics D: Applied Physics, **52**, 395502 (2019). https://doi.org/10.1088/1361-6463/ab2d5b

[40] Hui L., Schadler L. S., Nelson J. K.: The influence of moisture on the electrical properties of crosslinked polyethylene/silica nanocomposites. IEEE Transactions on Dielectrics and Electrical Insulation, **20**, 641–653 (2013). https://doi.org/10.1109/TDEI.2013.6508768

[41] Idumah C. I., Obele C. M.: Understanding interfacial influence on properties of polymer nanocomposites. Surfaces and Interfaces, **22**, 100879 (2021). https://doi.org/10.1016/j.surfin.2020.100879

[42] Raetzke S., Kindersberger J.: The effect of interphase structure in nanodielectrics. IEEJ Transactions on Fundamentals and Materials, **126**, 1044–1049 (2006). https://doi.org/10.1541/ieejfms.126.1044

[43] Popov I., Carroll B., Bocharova V., Genix A-C., Cheng S., Khamzin A., Kisliuk A., Sokolov A. P.: Strong reduction in amplitude of the interfacial segmental dynamics in polymer nanocomposites. Macromolecules, **53**, 4126–4135 (2020). https://doi.org/10.1021/acs.macromol.0c00496

[44] Grande C. D., Mangadlao J., Fan J., de Leon A., Delgado-Ospina J., Rojas J. G., Rodrigues D. F., Advincula R.: Chitosan cross-linked graphene oxide nanocomposite films with antimicrobial activity for application in food industry. Macromolecular Symposia, **374**, 1600114 (2017). https://doi.org/10.1002/masy.201600114

[45] Chen T-H., Chen Y-R., Chen L-H., Chang K-S., Lin Y-F., Tung K-L.: Exploration of the nanostructures and separation properties of cross-linked mixed matrix membranes using multiscale modeling. Journal of Membrane Science, **543**, 328–334 (2017). https://doi.org/10.1016/j.memsci.2017.08.061

[46] Lyn F. H., Peng T. C., Ruzniza M. Z., Hanani Z. A. N.: Effect of oxidation degrees of graphene oxide (GO) on the structure and physical properties of chitosan/GO composite films. Food Packaging and Shelf Life, **21**, 100373 (2019). https://doi.org/10.1016/j.fpsl.2019.100373

[47] Srinophakun T., Martkumchan S.: Ionic conductivity in a chitosan membrane for a PEM fuel cell using molecular dynamics simulation. Carbohydrate Polymers, **88**, 194–200 (2012). https://doi.org/10.1016/j.carbpol.2011.11.094

[48] Zhang H-P., Gandhi N. S., Gu Y., Zhang Y., Tang Y.: Chitosan/graphene complex membrane for polymer electrolyte membrane fuel cell: A molecular dynamics simulation study. International Journal of Hydrogen Energy, **45**, 25960–25969 (2020). https://doi.org/10.1016/j.ijhydene.2020.03.124

[49] Yan K. Y., Xue Q. Z., Zheng Q. B., Hao L. Z.: The interface effect of the effective electrical conductivity of carbon nanotube composites. Nanotechnology, **18**, 255705 (2007). https://doi.org/10.1088/0957-4484/18/25/255705

[50] Prokhorov E., Barquera-Bibiano Z., Manzano-Ramírez A., Luna-Barcenas G., Kovalenko Y., Hernández-Landaverde M. A., Castillo Reyes B. E., Hernández Vargas J.: New insights in graphene oxide dielectric constant. Materials Research Express, **6**, 085622 (2019). https://doi.org/10.1088/2053-1591/ab22f0

[51] Campbell S. L., Chancelier J. P., Nikoukhah R.: Modeling and simulation in Scilab/Scicos. Springer, New York (2006).